Phys. Chem. Glasses: Eur. J. Glass Sci. Technol. B, April 2006, **47** (2), 110–120

Invited paper

Recent advances in ion exchanged glass waveguides and devices

Seppo Honkanen, Brian R. West, Sanna Yliniemi, Pratheepan Madasamy, Michael Morrell, Jason Auxier, Axel Schülzgen, Nasser Peyghambarian, James Carriere, Jesse Frantz, Ray Kostuk

Optical Sciences Center, University of Arizona, Tucson, AZ 85721, USA

Jose Castro & David Geraghty

Department of Electrical and Computer Engineering, University of Arizona, Tucson, AZ 85721, USA

Ion exchange in glass is a well established method for fabrication of passive and active integrated photonic devices. For passive devices, the main advantages of ion exchanged waveguides are very low propagation losses, excellent mode matching to optical fibre and low waveguide birefringence that can all be achieved with a relatively simple fabrication process. For waveguide lasers and amplifiers, the ion exchange process is superior due to the compatibility with glass substrates having high rare earth ion concentrations. In this paper, we review the recent advances in the field of ion exchange glass waveguide technology with the emphasis on the results of our research group. We describe an advanced design and modelling tool for ion exchanged glass waveguides and present results on various passive and active waveguides and devices.

1. Introduction and review

The process of ion exchange in glass has been known for well over a millennium. In large doses, ions introduced into a glass matrix will form metallic clusters. The type of ion and size distribution of the particles produces a spectral attenuation in the glass, giving it a characteristic colouring. The aesthetic properties of ion exchanged glass were known to Egyptians of the sixth century, who used the process to colour glazed earthenware,[1] and the technique is also known to have been applied to the staining of window glass in the middle ages. Ion exchange as an engineering process was originally used to improve the surface mechanical properties of structural glass.[2–4] As glass fails in tension, the introduction of a compressive stress at the surface will increase the modulus of rupture. This can be accomplished by exchanging sodium ions in the glass with ions of greater size, such as silver (the process is often termed 'ion stuffing'). Interestingly, this concept has recently found photonics applications, increasing the thermal shock resistance of laser glasses.[5]

The fabrication of optical waveguides in glass by ion exchange was first achieved in 1972 using a melt containing thallium ions.[6] The Tl^+–Na^+ system was problematic due not only to the mild toxicity of Tl^+, but also to the large index change (~0·1), which causes difficulty in repeatably producing single-mode waveguides. Subsequently, Giallorenzi *et al*[7] produced waveguides using a melt containing silver ions, which today is by far the most common process. Other dopant ions include Cs^+, Rb^+, K^+, and Li^+.[8]

The creation of integrated optical devices (also referred to as 'planar lightwave circuits', due to the planar processing techniques used to fabricate them) in glass offers several obvious benefits over other technologies. Intrinsic absorption is very low in the near infrared region of the spectrum. Coupling losses to optical fibre are minimised due to the similarity in refractive index. In addition, glasses are amorphous, meaning that they exhibit no intrinsic material birefringence, unlike crystalline semiconductors. This is not to say that birefringence is not an issue in glass waveguides – both the shape of the waveguide and the stresses that arise during fabrication contribute to birefringence, but with proper design, these can be balanced against each other to produce single-mode devices with very low polarisation dependence.[9]

In addition to ion exchange, other processes exist through which glass waveguides have been fabricated. Most involve the deposition of thin glass films (e.g. chemical vapour deposition, flame hydrolysis deposition, sol-gel coating), followed by reactive ion etching to define the device geometry, and subsequent deposition of the overcladding. The multiple deposition steps and etching make these methods costly and time consuming. The benefits of ion exchange over competing glass based technologies

Paper presented at the American Ceramics Society Glass and Optical Materials Division (GOMD) Fall Meeting and 14th International Symposium on Non-Oxide Glasses, Florida, USA. 7–12 November 2004.
[1] Corresponding author. Email address: seppo@optics.arizona.edu

are numerous. Ion exchanged waveguides possess many desirable characteristics. It is very easy to make waveguides exhibiting very low propagation losses of less than 0·1 dB/cm. The increase in refractive index between the waveguide and the substrate is relatively small, allowing for easy fabrication of single-mode waveguides, and excellent mode matching to single-mode fibre can be achieved through a technique of waveguide burial. Ion exchanged waveguides can exhibit very low birefringence across a broad range of waveguide widths.[10] This is critical for certain resonant devices[11] and devices that contain both single- and multimode waveguides.[12] The process is cost effective, requiring no complicated material growth steps following the photolithography that is common to all processes. Finally, it is tolerant to imperfections in the photolithography – edge roughness in the mask that defines the waveguide geometry is rendered less damaging due to the diffusive nature of the ion exchange.

The applications of integrated optics extend far beyond the telecommunications industry. One rapidly emerging field of study is the design of integrated optical sensors, in which a guided wave interacts with the environment, causing a perturbation of the optical field. For sensor applications, glass based devices have a distinct advantage over those fabricated in semiconductors or inorganic crystals such as $LiNbO_3$. Regardless of whether the sensor operates on refractometry or absorption, sensitivity is proportional to the overlap of the guided mode with a sensitised superstrate. Depending on the measurand, this layer is commonly based on organic compounds having an index of around 1·4–1·6, or an aqueous solution with an index near 1·33. These indices are very close to that of glass (n~1·5). The small dielectric barrier between the glass and the superstrate results in a large mode overlap, maximising the sensitivity.[13] In contrast, the higher indices of $LiNbO_3$ (n=2·2 @ 633 nm) and semiconductors (n>3) greatly reduce the influence of the superstrate. Of all glass waveguide technologies, ion exchange holds the most potential for sensor applications due to its low cost. Unlike telecommunications devices, many sensors are designed to be disposable.

With the introduction of the erbium doped fibre amplifier (EDFA) and the resulting importance of wavelength division multiplexed (WDM) telecommunication systems, there has been a recent emphasis on the development of glass-based devices that operate in the 1·55 μm wavelength range. Such devices include y-branches,[14] Mach-Zehnder interferometers,[15] and ring resonator gyroscopes.[16] The observation of ultraviolet photosensitivity in some glasses used for ion exchange[17] has supported the successful production of grating based devices.[18,19] Furthermore, the recently reported success in forming waveguides by ion exchange in quantum dot doped glass shows promise for nonlinear device applications.[20]

The ion exchange process has been utilised for the production of active devices as well. The earliest such devices were splitters that included an amplifying region to compensate for the splitting loss.[21] One tremendous benefit of ion exchange over semiconductor based processes is the presence of hybrid substrates, glass wafers that consist of active and passive sections that have been joined together in the same plane.[22] In semiconductor processes, fabricating such a waveguide usually requires regrowth techniques.

Ion exchanged waveguide amplifiers have been extensively investigated and very impressive results demonstrated (Teem Photonics, www.teemphotonics.com). However, they have achieved little practical success. Two major factors contribute to this. First, the short length of waveguide devices requires an extremely high gain per unit length in order to compete with fibre amplifiers. This necessitates a high concentration of rare earth ions within the glass, which eventually leads to a decrease in pumping efficiency due to cooperative upconversion. Second, unlike rare earth doped fibre, which has radial concentration and index profiles that are optimised for pump/signal/gain medium overlap, waveguides that are ion exchanged into a homogeneously doped substrate exhibit a relatively poor overlap, decreasing the gain. Waveguide amplifiers do have an advantage over their fibre based counterparts, nonetheless, in that the passive elements (pump–signal combiner, tap coupler for power monitoring, etc.) can be integrated onto the same substrate as the amplifier. Ion exchanged waveguide lasers, however, are becoming increasingly popular. High reflectivity dielectric mirrors or Bragg gratings can be used to provide a net round trip gain in ion exchanged Yb^{3+}/Er^{3+}-doped waveguides of a few centimetres in length, leading to single longitudinal mode lasing.[23] Alternatively, the feedback may be provided by a grating etched directly into the active substrate.[24,25]

In the following sections, we first describe the different ion exchange configurations used in channel waveguide fabrication by using Ag^+–Na^+ exchange process as an example. Then we briefly describe an advanced modelling software that we have developed[26] and show examples of our recent experiments on different types of channel waveguides. Section 5 gives a brief review of the recent device experiments of the ion exchange team at the University of Arizona. Finally in Section 6 we will give a short summary.

2. Ion exchange processes

Previous authors have identified no fewer than seven different processing configurations for ion exchange,

which are summarized in Ref. 27. Of these, a sequence consisting of thermal exchange from a molten salt, with or without the presence of an applied electric field, followed by field-assisted burial and thermal annealing, has been shown to produce waveguides with the aforementioned desirable properties.

All ion exchange processes are described here as they pertain to the silver-sodium (Ag^+–Na^+) system of ions. Figure 1(a) illustrates the thermal exchange from a molten salt source through a metal-oxide mask. The mask is used to define the device geometry for the exchanges from molten salt. Ag^+ ions are driven into the substrate from the melt by a chemical potential gradient, and in order to preserve charge neutrality, Na^+ ions are released into the melt. Once in the glass phase, Ag^+ ions are redistributed by thermal diffusion. The dielectric mask serves to reduce the occurrence of metallic silver clusters which would otherwise form due to electrolytic deposition at the glass/mask interface.[28] Such clusters produce a spectral attenuation in the waveguides.

Thermal exchange may also be assisted by an applied electric field. A voltage V_a is applied across the substrate of thickness d, with the anode plane at the masked surface, as shown in Figure 1(b). Under the influence of the resulting electric field, the Ag^+ ions migrate deeper into the glass than they would in a purely diffusive process, and achieve a step like profile under the mask. This process is preferred when a buried waveguide requires high optical confinement.

The field assisted burial process step is shown in Figure 1(c). The substrate is placed in a melt containing Na^+ ions. A voltage V_a is applied across the substrate, as with the field assisted thermal exchange. As the Ag^+ ions migrate deeper into the glass, they are replaced by Na^+ ions near the surface. Burial of the waveguide is beneficial in several ways. Reduction of the optical mode overlap with the substrate surface decreases propagation loss (which is caused by surface scattering), and birefringence (which arises due to the asymmetric boundary condition of the dielectric constant). Furthermore, the buried guide can be made to have nearly circular symmetry, which improves coupling efficiency to optical fibre.

Figure 1(d) illustrates the process step of thermal annealing. No external ion source or applied field is present, so the existing Ag^+ ions are redistributed entirely through thermal diffusion at an elevated temperature. This process provides for fine adjustment of the mode shape and birefringence.

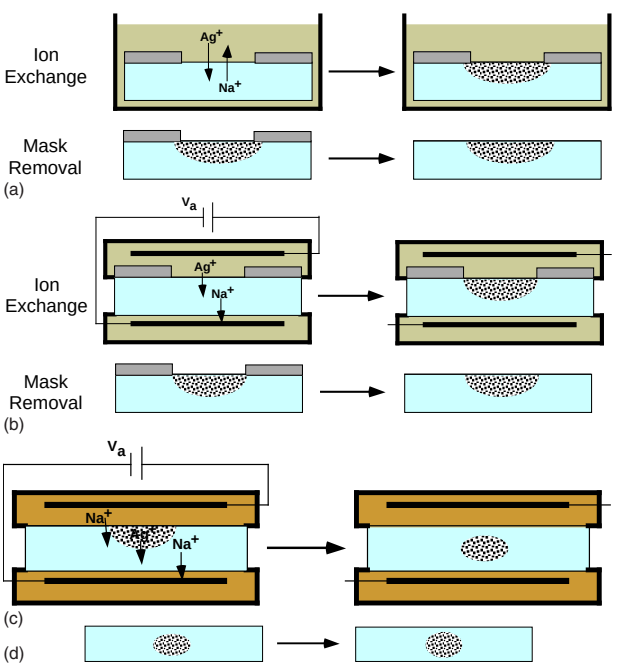

Figure 1. The four most common processing configurations for ion exchange. (a) thermal exchange from a molten salt. (b) field assisted exchange from a molten salt. (c) field assisted burial. (d) thermal annealing

3. Modelling of ion exchanged channel waveguides

3.1 Process modelling

The time evolution of silver ion concentration is derived in Ref. 29:

$$\frac{\partial C_{Ag}}{\partial t} = \frac{D_{Ag}}{1-(1-M)C_{Ag}}\left[\nabla^2 C_{Ag} + \frac{(1-M)\left(\nabla C_{Ag}\right)^2}{1-(1-M)C_{Ag}} - \frac{q\vec{E}_{ext}.\vec{\nabla}C_{Ag}}{kT}\right] \quad (1)$$

where, D_{Ag} and D_{Na} are the self diffusion coefficients of silver and sodium ions, respectively, and M=D_{Ag}/D_{Na} is their ratio. C_{Ag} is the concentration of Ag^+ ions, normalised with respect to the saturated concentration. The saturated concentration is dependent on the stoichiometry of the substrate and melt. Its exact value is generally unknown, but this problem is overcome by setting C_{Ag}=1 at the surface and using a corresponding value for the index increase Δn_0 at the surface (see Equation (2)) that is determined experimentally. E_{ext} is the applied electric field, which is modelled as described below. T, k, and q are the absolute temperature, Boltzmann's constant, and the electron charge, respectively. The first term on the right hand side of Equation (1) is the contribution to $\partial C_{Ag}/\partial t$ arising from the concentration gradient of the Ag^+ ions. The second term arises from the internal electric field due to the local distribution of dissimilar ions. When there is an externally applied field, as in the field assisted burial step, the third term representing ion drift must be included as well.

Solving Equation (1) subject to the boundary conditions listed in Table 1 produces the Ag^+ concentration profile. The nonlinear Equation (1) has no

analytical solution and a general solution requires numerical methods. In our model we employ the alternating direction implicit method of Peaceman & Rachford (PR-ADI).[30] This combines the computational efficiency of explicit methods and the stability of implicit methods. Each time step is divided into two half steps. In the first, partial derivatives are calculated explicitly with respect to one dimension, and implicitly with respect to the other. The process is then reversed for the second half step.

The boundary conditions on potential φ are slightly more complicated than those for ionic concentration. Realising that only the spatial derivatives of potential are required to solve Equation (1), we set φ=0 at the bottom of our simulation domain (y=h) and φ=U at the surface (y=0), where U=$V_a h/d$. At the sides of the domain, $|x|$=W/2, we apply the Neumann condition $\partial\varphi/\partial x$=0. This requires that the side and bottom boundaries of the domain are sufficiently far from the waveguide that ionic conductivity is homogeneous at the boundary.

Field modelling becomes more complicated when the field is applied through a mask. This situation arises during the field-assisted thermal exchange from melt, as shown in Figure 1(b). Furthermore, some applications require that the waveguide burial process be asymmetric in the x-direction.[31,32] In this case, a second mask is deposited onto the substrate following the initial thermal exchange. This mask has both open and closed regions within the simulation domain. As it is not possible for incoming Na^+ ions to penetrate the mask during burial, a space charge layer builds up directly underneath the mask to compensate for the electric field. Effectively, the mask acts as an electrical insulator. For these 'selective' field assisted processes, the boundary condition on electrical potential at the surface is modified to force $\partial\varphi/\partial y$=0 in the masked regions. The boundary conditions for both full and selective burial are shown in Table 2.

To a first approximation, the electric field present during the full burial step is simply the voltage drop across the substrate divided by the substrate thickness. However, the conductivity of the glass is inhomogeneous in the region of the waveguide, owing to the differing conductivities of the two ionic species. The result is a perturbation of both the magnitude and direction of the electric field lines in the vicinity of the waveguide. The field modelling procedure taking also the inhomogeneous conductivity into account is described in Ref. 26.

Table 1. Boundary conditions on Ag^+ concentration used in ion exchange modeling

Process step	*Surface (y=0)*		*Bottom of domain (y=h)*	*Sides of domain ($\|x\|$=W/2)*
Thermal exchange from molten salt	C_{Ag}=1 $\partial C_{Ag}/\partial y$=0	(mask open) (mask closed)	C_{Ag}=0	C_{Ag}=0
Field-assisted burial: full	C_{Ag}=0		C_{Ag}=0	C_{Ag}=0
Field-assisted burial: selective	C_{Ag}=0 $\partial C_{Ag}/\partial y$=0	(mask open) (mask closed)	C_{Ag}=0	C_{Ag}=0
Annealing	$\partial C_{Ag}/\partial y$=0		C_{Ag}=0	C_{Ag}=0

3.2 Optical modelling

To model the optical properties of an ion exchanged waveguide, we must first convert the Ag^+ concentration profile to a refractive index distribution. The presence of Ag^+ ions locally perturbs the index via three physical mechanisms; ionic size, ionic polarisability, and induced stress. The stress-induced index change is relatively small in Ag^+–Na^+ exchange and is complicated to take accurately into account. We will concentrate on the other two contributions. A basic model predicts that both of them produce local changes in refractive index that are linearly proportional to the Ag^+ concentration, and thus it is not necessary explicitly to separate the two effects.

The refractive index profile of the waveguide cross section can be expressed as

$$n(x,y,\lambda)=n_{sub}(\lambda)+\Delta n_o(\lambda)C_{Ag}(x,y) \quad (2)$$

where $n_{sub}(\lambda)$ is the substrate index before ion exchange and $\Delta n_o(\lambda)$ is the increase in refractive index resulting from C_{Ag}=1, determined experimentally.

The electric field E_n of each scalar mode supported by the waveguide is found by solving the Helmholtz equation

$$(\nabla^2+k^2)E_n=\beta_n^2 E_n \quad (3)$$

where k=$k_o n(x,y)$=$2\pi n(x,y)/\lambda$ is the wavenumber and β_n is the propagation constant of the nth mode. While the scalar modes are useful in determining such waveguide characteristics as burial depth and waveguide-to-fibre coupling efficiency, modelling of birefringence requires that the individual components $E_{TE,n}$ and $E_{TM,n}$ of each mode be evaluated, with

$$\Delta n_n = \frac{1}{k_o}\left(\beta_{TE,n}-\beta_{TM,n}\right). \quad (4)$$

A semivectorial finite difference method intro-

Table 2. Boundary conditions on potential used in electric field modelling

Process step	*Surface (y=0)*		*Bottom of domain (y=h)*	*Sides of domain ($\|x\|$=W/2)*
Full burial	φ=U		φ=0	$\partial\varphi/\partial x$=0
Selective burial or field-assisted thermal exchange	φ=U $\partial\varphi/\partial y$=0	(mask open) (mask closed)	φ=0	$\partial\varphi/\partial x$=0

duced in Ref. 33 and extended to variable node spacing in Ref. 34 is employed to solve Equation (3) with the appropriate discontinuity conditions of the normal field components.

To illustrate the accuracy of our modelling software, we designed a two-mode waveguide to be fabricated in a Schott-BGG31 substrate (50 mm in diameter). For predetermined process parameters, we used slab waveguide experiments and prism coupler measurements to extract the following glass parameters for the first process step (thermal ion exchange at 553 K): D_{Ag}=1·1×10^{-15} m^2/s , M=0·72, and Δn_0=0·0340 (at 1550 nm wavelength). At the burial temperature of 528 K the value of D_{Ag}=5×10^{-16} m^2/s was determined. The duration of the first step was 60 min and we used 5 μm mask opening. The duration of the burial step was 5 min with an applied voltage of 275 V across a 2 mm thick substrate. Figure 2 shows the modelled and measured mode intensity profiles for the even and odd mode of this two mode waveguide. The modes of the fabricated waveguide were selectively excited using an adiabatic mode combiner.[19] Next, a grating was written into the two mode waveguide by exposing the substrate to ultraivolet irradiation through a phase mask. Based on the measured Bragg wavelengths, the effective indices were determined. The measured effective indices are 1·4637 and 1·4575 and the modelled ones are 1·4638 and 1·4575. The discrepancy is only 10^{-4} – which is well within the limits of both measurement and processing uncertainty (the change in effective index change due to the grating, for instance, is on the order of 10^{-4}).

4. Channel waveguide experiments

4.1 Burial depth of waveguides with different widths

In many devices, there is a need to use waveguides of different widths at different sections of an integrated optical circuit. Examples of such devices are arrayed waveguide gratings (AWGs)[12] and devices based on multimode interference (MMI).[35] If these devices are fabricated using buried ion exchanged waveguides, significant losses are expected due to vertical waveguide misalignment at the junction between two waveguides having different widths. This is due to the fact that the burial depth is different for a channel waveguide and a slab waveguide having no lateral confinement.

We investigated the burial depth dependence on the waveguide width by fabricating buried waveguides in Schott-BGG31 glass (75 mm in diam-

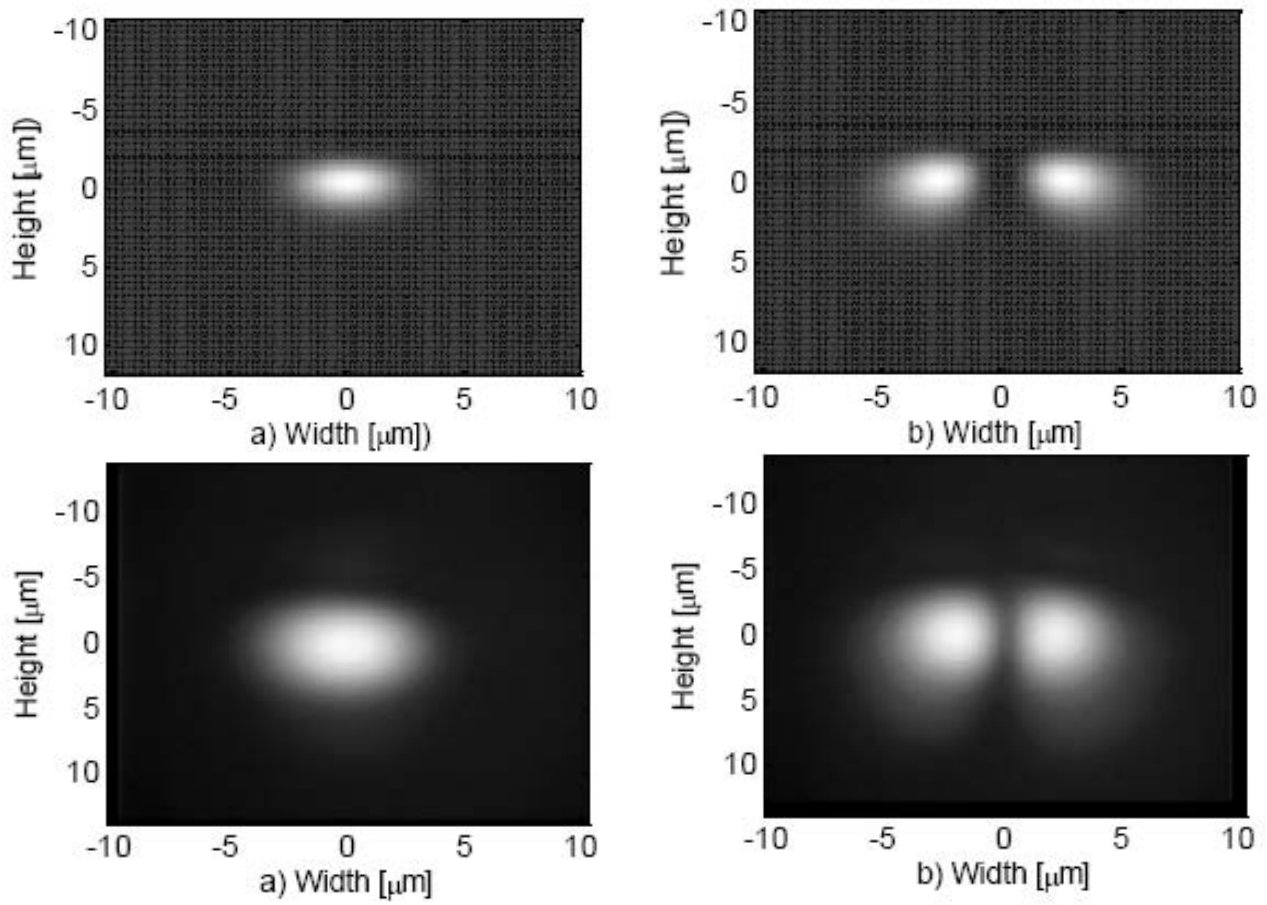

Figure 2. (a) Modelled mode intensity profiles of the two-mode waveguide. (b) Measured mode intensity profiles of the two-mode waveguide

eter) using mask opening widths ranging from 2–9 μm.[36] The burial depth of the waveguide is defined in terms of the mode profile since that is more relevant in practical applications. The first step, thermal ion exchange, was performed in a 50:50 $AgNO_3/NaNO_3$ melt at T=553 K for 4500 s. The second step, an unmasked field assisted burial, was done at T=523 K for 2400 s with an applied voltage of 320 V across a 2 mm substrate thickness. To model these buried waveguides we used the following glass parameters: The self diffusion coefficient for Ag^+ ions of 1×10^{-15} m^2/s at T=553 K and $3{\cdot}5\times10^{-16}$ m^2/s at T=523 K, M value of 0·2 and the maximum index change of 0·03 at the glass surface. The parameters were extracted from slab waveguide experiments and by using prism coupler measurements. The experimental results are plotted in Figure 3 and they agree well with the modelling results for M=0·2. The figure also shows the modelling results for M values of 0·5 and 1 (keeping the self diffusion coefficient for Ag ions the same). As expected, the burial depth dependence on waveguide width decreases with increasing value of M and vanishes completely when Ag and Na ions have equal self diffusion coefficients.

4.2 Birefringence of buried waveguides

We also investigated the birefringence of buried waveguides having different widths.[10] The measured birefringence values for the fundamental waveguide modes, defined as N_{eff}(TE-mode)–N_{eff}(TM-mode), as a function of a mask opening width are shown in Figure 4. These very low values clearly demonstrate one of the most attractive features of ion exchanged waveguides, i.e. negligible birefringence. The values without post annealing are on the order of 10^{-5} for all mask opening widths. The modelling resulted in about 5×10^{-6} or larger values for the birefringence. These slightly larger values are due the fact that our model does not take the stress induced index increase into account, which is larger for TM modes compared to TE modes. The birefringence increases as a function of a mask opening width, since the wider waveguides are more elliptical increasing the form birefringence, while the stress induced birefringence has much smaller dependence on waveguide width.

The ellipticity of the waveguide can be significantly reduced by post annealing. During the annealing, Ag^+ ions further diffuse and the waveguides become more circular. The more the sample is annealed the smaller the form birefringence becomes and at some point the stress induced birefringence becomes dominant. Eventually the sign of the birefringence is changed as demonstrated in Figure 5. With proper annealing, extremely low birefringence can be achieved for waveguides width broad range of widths.

4.3 Quantum dot doped channel waveguides

One of the strengths of ion exchange technology is that it is well suited for active devices, which have gained a lot of attention recently. We have studied ion exchanged waveguides in semiconductor doped glasses[20] that have several advantages over their epitaxially grown counterparts. Doped glasses are easier and less expensive to fabricate than structures grown through epitaxial techniques. Suitable thermal treatment of a glass containing the chemical components of a semiconductor can precipitate semiconductor quantum dots (QDs) with narrow size distributions, few substitutional defects, and few dangling bonds. The 3D quantum-confinement of the semiconductor QDs allows us to tailor the optical absorption. These properties make QD-doped glass an attractive candidate for the production of nonlinear photonic devices.

The PbS QDs studied here have radii (2–5 nm) smaller than the bulk exciton Bohr radius (18 nm), which places them within the strong 3D-confinement limit. The small bulk bandgap energy (0·4 eV @ 300 K) allows us to tune the ground excited

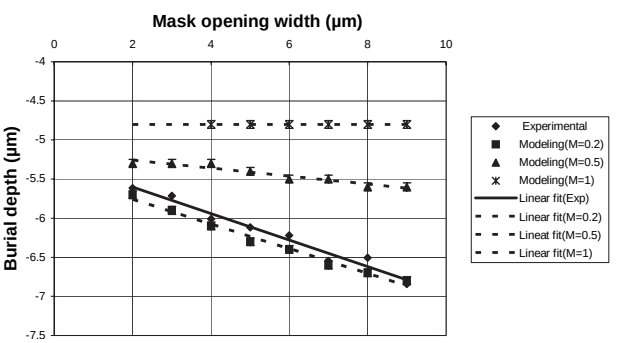

Figure 3. The burial depth variation as a function of mask opening width. The solid line corresponds to the linear fit for the experimental data and the dashed lines correspond to the linear fit for the modelled data

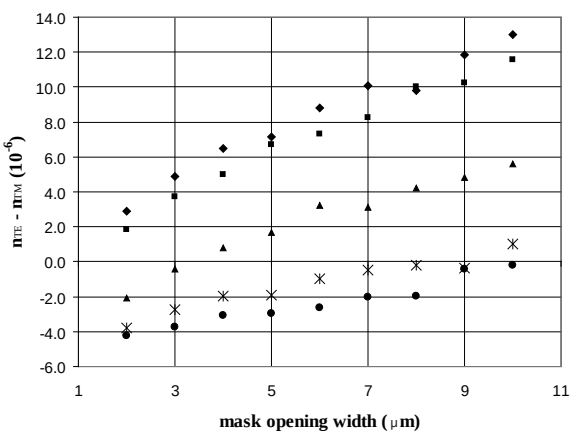

Figure 4. Birefringence ($n_{TE} - n_{TM}$) before annealing (diamonds) and after annealing at 250°C for 15 min (squares), 45 min (triangles), 75 min (crosses), 105 min (dots)

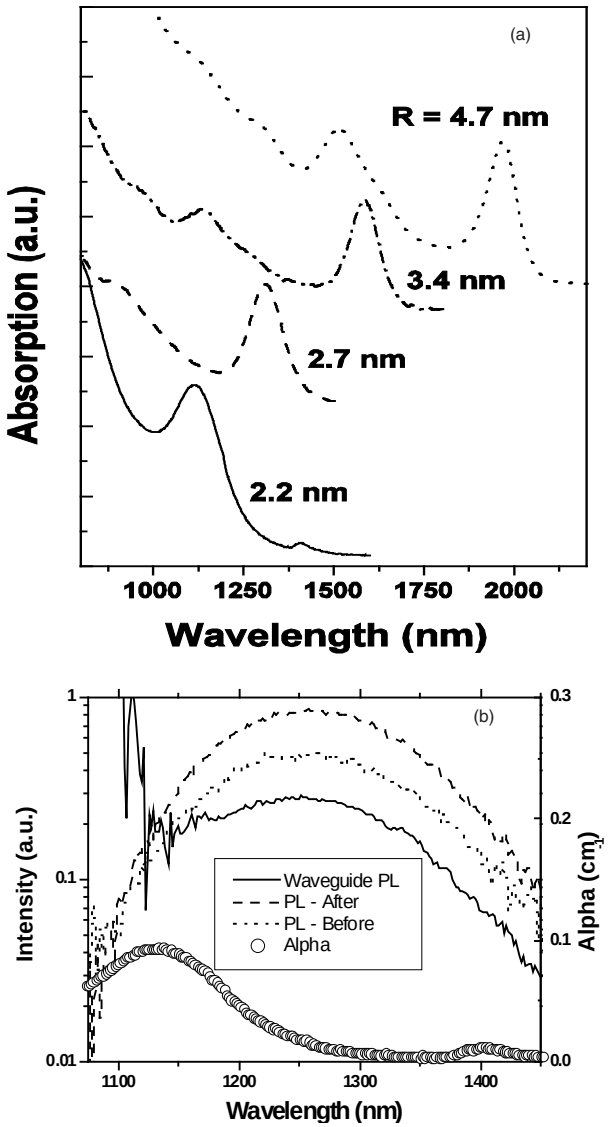

Figure 5. (a) Room temperature absorption spectra of PbS QD-doped glasses with mean QD radii R. The solid line (R=2·2 nm) represents the sample in which the ion-exchange waveguides have been fabricated. (b) Luminescence from PbS QD-doped waveguides (solid line) and in this glass before (dotted line) and after (dashed line) ion exchange along with QD absorption (open circles)

state transition throughout the near infrared, which includes telecommunications wavelengths (1300 and 1550 nm). Figure 5(a) shows the room temperature absorption spectra of PbS QD-doped glasses with different dot radii.

We first tried Ag^+–Na^+ ion exchange for channel waveguide fabrication. However, metallic silver nanocrystal formation within the glass resulted in lossy waveguides. Due to the high loss in these silver ion exchanged waveguides, we investigated K^+–Na^+ ion exchange. At a given temperature, the self diffusion coefficient of K^+ ions is several orders of magnitude smaller than that of Ag^+ ions. By increasing the temperature and exchange times, we were able to produce low loss surface channel waveguides using a pure KNO_3 salt melt. Excluding the absorption due to quantum dots, we measured a guide loss of <0·5 dB/cm for our QD-doped channel waveguides.

These waveguides not only provide optical confinement, but they are semi-homogeneously doped with PbS QDs. Figure 5(b) shows luminescence from samples with and without ion exchange and from an ion exchanged waveguide. There is no noticeable difference between these spectra, which demonstrates that the optical properties of the quantum dots remain unchanged through the ion exchange process.

5. Device demonstrations

5.1. Add-drop wavelength filter

In a point-to point dense wavelength division multiplexing system (DWDM), multiple wavelengths are coupled into optical fibre by a wavelength multiplexer at the transmitter end. At the receiver end, those wavelengths are fanned out by a wavelength demultiplexer. This point-to-point fibre optic network forms the backbone of the DWDM transmission system. Wavelength add/drop filters are required to have access to the individual wavelengths at any point of the system. The difference between a demultiplexer and an add/drop filter is that the add/drop filter not only has the function of demultiplexing, but also has the function of wavelength routing or coupling. It can drop (or add) the required one wavelength from (or to) the fibre network without affecting the transmission of other wavelengths. A wavelength channel add/drop filter is a key device in fibre optical networks.

The device we have proposed for this application is an ion exchanged waveguide add/drop wavelength filter[18] shown schematically in Figure 6(a). Two buried single mode waveguides of different widths are brought together adiabatically into a two mode section. The two mode section is later separated again into the two single mode waveguides. Bragg gratings are ultraviolet written at a small angle in the two mode section. The filter functions as follows: input signals on the narrow waveguide are coupled to the odd mode of the two-mode section. For wavelengths on resonance, a tilted grating breaks the orthogonality of the two modes and reflects the signal to the backwards propagating even mode. This propagates back out of the wide 'drop' port. Wavelengths off resonance pass through the Bragg grating and continue on to the narrow output port. Additionally, a signal on resonance at the dropped wavelength can be added through the fourth port. A fabricated device yielded excellent results (see Figure 6(b) with a 20 dB extinction ratio and a 0·4 nm 3 dB bandwidth. More recently, we have performed a detailed theoretical and experimental analysis of our

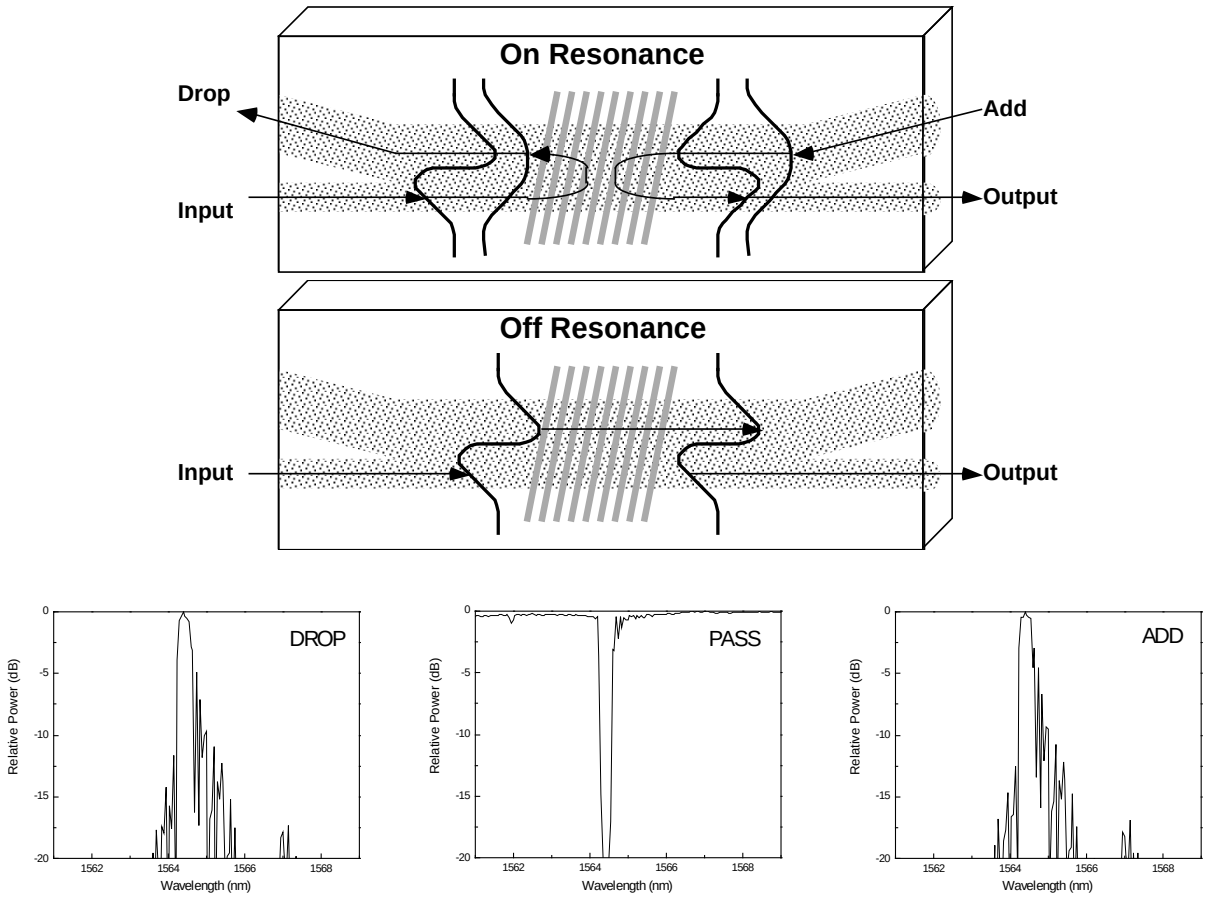

Figure 6. (a) Schematics of the add/drop wavelength filter. (b) The measured performance of a fabricated device

add/drop devices.[19] The theoretical analysis includes the ion exchange modelling, optical modelling of the waveguides, grating modelling and full analysis of the device. The theoretical results are in excellent agreement with the experiments.

5.2. Er-doped waveguide lasers

Perhaps the most attractive recent use of ion exchanged waveguides is to employ them in an Er-doped glass substrate, with the goal to develop compact glass waveguide amplifiers and lasers for 1550 nm wavelength region. We have investigated the use of an Ag film ion exchange technique for fabrication of waveguide lasers in Er-doped phosphate glass.[37,23] The first process step introduces Ag^+ ions in the glass just beneath the surface, where they replace Na^+ ions and locally increase the refractive index of the glass, thus forming a waveguide. In contrast to conventional ion exchange processes using molten salts as ion sources a thin silver film is used as an ion source in Ag film ion exchange. The silver ions are released from the film and driven into the glass with an electric field. The second step of the process is a simple thermal annealing to modify the waveguide profile. Compared to the molten salt ion exchange processes the Ag film ion exchange has its unique advantages, especially when a 'difficult' substrate such as a phosphate glass is used. Phosphate glasses are preferred for erbium doped waveguide amplifiers (EDWA) and lasers because of the high solubility of rare earth ions in phosphate glasses, which allows doping high erbium concentrations without significant lifetime reduction. However, phosphate glasses react easily with molten salt baths and etchants used to remove the diffusion mask, resulting in damage to the surface. Also, hybrid substrates containing active and passive regions are required when active and passive devices are integrated monolithically in a single substrate. Molten salt baths can easily damage the joint between the active and passive regions. Therefore a gentle waveguide fabrication process, which does not damage the surface of the glass nor the joint between the active and passive regions, is preferred. This will ensure low propagation losses and allows repeatable subsequent photolithographic processing of the glass, e.g. for fabrication of DBR gratings for waveguide lasers.

We have demonstrated that Ag film ion exchange is a gentle technique without the use of salt melts or strong etchants and causes no damage to the surface of phosphate glass. High quality surface waveguides can be fabricated in rare earth doped phosphate glasses. The process can be performed at

low temperatures and a photoresist can be used as a diffusion mask. The use of a photoresist as a mask makes the channel waveguide patterning as simple and accurate as possible.

We have recently developed the process to fabricate Ag film ion exchanged waveguides in commercially available Schott IOG-1 phosphate glass, which is doped with very high concentrations of erbium and ytterbium. Typical doping levels are 1·15 wt% Er_2O_3 ($1·0\times10^{20}$ ions/cm^3) and 4·73 wt% Yb_2O_3 ($4·0\times10^{20}$ ions/cm^3). For single mode channel waveguides the mask aperture widths in the photoresist range from 2–10 μm and the ion exchange is done at ~100°C for about 1 h with a voltage of ~100 V. After removing the remaining silver film and resist, the glass substrate is annealed at ~230°C for about 2 h. The propagation losses of our waveguides are ~0·15 dB/cm.

Multi wavelength laser arrays can conveniently be fabricated by using a simple surface relief grating and varying the width of waveguides in the array. These were first demonstrated by molten salt potassium ion exchange.[24] The wavelength range demonstrated was only about 0·3 nm (less than 50 GHz) due to the low index change resulting from potassium ion exchange. Our group recently demonstrated that the use of Ag film ion exchange in this type of a DBR waveguide laser array can result in much broader wavelength range (covering six ITU grid wavelengths).[37] Molten salt silver ion exchanged multiwavelength DFB laser arrays based on the same idea have also been demonstrated.[25]

A schematic diagram of our waveguide laser array is shown in Figure 7(a). The laser cavity is implemented with a broad band high reflection dielectric mirror on one end and a surface relief grating on the other end. An array of lasers lasing at different wavelengths can be fabricated by changing the width of the waveguides and keeping the period of the grating the same. The effective index of the waveguide depends on the width of the waveguide, which changes the Bragg wavelength. By controlling the width of the waveguides, each channel can be designed to lase at different ITU (International Telecommunication Union) specified wavelengths. The number of wavelengths that can be implemented with a single grating depends on the maximum index change that can be obtained by the fabrication process. Our Ag film ion exchange has the advantage of producing a larger index change compared to molten salt processes. The surface relief gratings in our lasers were fabricated holographically on the photoresist at the surface of the glass and then transferred into glass by Argon ion milling. Figure 7(b) shows the measured performance for the 5 μm wide waveguide at 1540·2 nm wavelength. For a coupled pump power (980 nm wavelength) of 145 mW, the output power was 11 mW with a threshold of 60 mW and a slope efficiency of

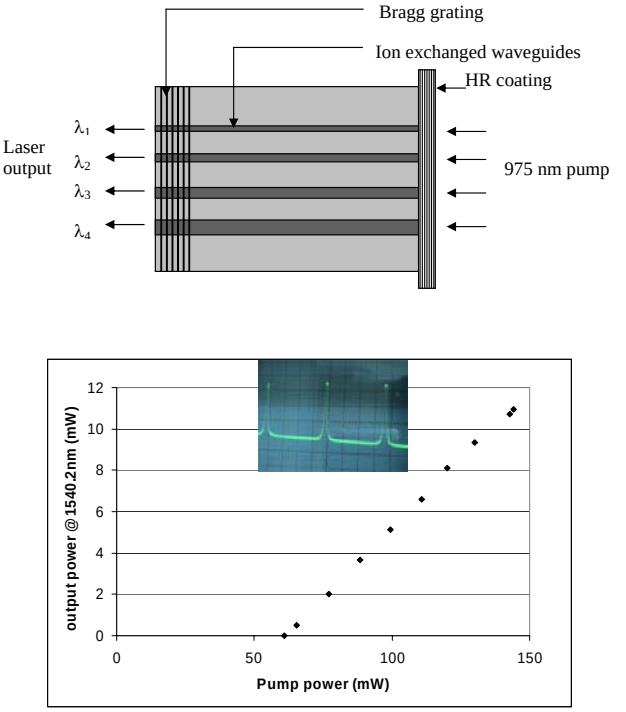

Figure 7. (a) Schematics of a DBR waveguide laser array implemented with a surface relief grating and a dielectric mirror on Ag film ion exchanged waveguides. (b) Laser output power as a function of pump power for a 5 μm waveguide. Inset shows the output from a scanning Fabry–Perot interferometer measurement

13%. The inset shows the output from a Fabry–Perot scanning interferometer measurement demonstrating single frequency operation. The resolution of our interferometer is 2·7 MHz, which is insufficient to measure the narrow linewidth of this laser.

In addition to the waveguide lasers using a single-mode pump laser diode, we recently proposed and demonstrated a novel erbium doped planar waveguide laser configuration, which enables easy pumping using low cost multimode semiconductor lasers.[23] The device was fabricated by Ag film ion exchange in a hybrid phosphate glass having Er-doped and passive regions monolithically integrated in a single substrate. To our knowledge this is the first successful device demonstration using the monolithic hybrid glass, which enables integration of active and passive ion exchanged devices in a single substrate. This feature is crucial for the success of active planar waveguide devices for fibre optic communications.

6. Summary

Ion exchange in glass has been used successfully for many years in the fabrication of waveguide devices. Accurate modelling and design of these devices has become more important as the complexity of the devices has increased and more exotic glass substrates are being used. Previous efforts at modelling

the process were simplistic at best, neglecting such important effects as conductivity variations within the waveguide and influence of the mask structure during electric field assisted process. In addition, previous models were based on algorithms that exhibited instability for commonly encountered vales of *M*. We have developed a model using the more stable Peaceman–Rachford alternating direction implicit algorithm to solve the two-dimensional binary diffusion equation describing ion exchange. Arbitrary mask configurations – and the resulting electric field profiles – are allowed, as is concentration dependent electrical conductivity in the region of the waveguide. To analyse properly the modelled waveguides, a semivector finite difference method was developed to calculate the mode fields and effective indices.

We have used our waveguide design model in connection with a variety of waveguide and device experiments, which have demonstrated an excellent agreement between theory and experiments. Our channel waveguide experiments show that the burial depth of ion exchanged waveguides depends on the waveguide width. This undesirable feature has to be taken into account when designing devices. Properly tapering the waveguides between sections of different widths should solve the problem in most cases. We have also demonstrated that extremely low birefringence in ion exchanged channel waveguides having different widths can easily be achieved, which is a highly attractive feature especially in telecommunications applications. Regarding the passive devices, we described an ion exchanged add/drop wavelength filter utilising an ultraviolet written grating. This filter is a good example of a device, in which low birefringence is required in waveguides with varying widths.

For our passive devices we have mostly relied on molten salt Ag^+–Na^+ ion exchange. However, in active devices employing doped substrates this process is not always the best choice. We have shown that K^+–Na^+ ion exchange gives excellent results in connection with quantum dot-doped glasses. With luminescence measurements we demonstrated that the optical properties of the quantum dots are not affected by the ion exchange process. Regarding Er-doped waveguide lasers using phosphate glass substrates, we have demonstrated that a dry Ag film ion exchange technique is an excellent choice. Using this process we have demonstrated novel high performance waveguide laser configurations.

To conclude, ion exchange in glass continues to be an important fabrication technology for planar photonic circuits. It has unique features, which makes it an attractive choice compared to other glass waveguide technologies. The low birefringence in passive devices is one of them. To fully benefit from the 'chip' scale integration, in future studies it will be beneficial to put emphasis on array devices. These could include arrays of dispersion compensators and all-optical packet header recognition devices.[38] As for the active devices, there are numerous possibilities in using rare earth and quantum dot-doped glasses as well as other even more exotic glass hosts.

Acknowledgements

Support from Arizona State Photonics Initiative (TRIF), NSF, Corning Inc. and BAE Systems is acknowledged. The collaboration with Nick Borelli on quantum-dot doped waveguides is greatly appreciated. The authors would also like to thank Joe Hayden, Jan Ingenhoff and Norbert Fabricius for many fruitful discussions.

References

1. Righini, G. C. Ion exchange process for glass waveguide fabrication. In *Critical Reviews of Optical Science and Technology*. Edited by S. I. Najafi, SPIE, Bellingham, WA, 1994, **Vol. CR53**.
2. Schulze, G. Versuche über die diffusion von silber in glas. *Angew. Physik*, 1913, **40**, 335–67.
3. Kistler, S. S. Stresses in glass produced by nonuniform exchange of monovalent ions. *J. Am. Ceram. Soc*., 1962, **45**, 59–68.
4. Zijlstrra, A. L. & Burggraaf, A. J. Fracture phenomena and strength properties of chemically and physically strengthened glass. *J. Non-Cryst. Solids*, 1968, **1**, 49–68.
5. Jiang, S., Myers, J. D., Wu, R., Bishop, G. M., Rhonehouse, D. L., Myers, M. J. & Hamlin, S. J. Chemically strengthened Er^{3+}, Nd^{3+} doped phosphate laser glasses. *Proc. SPIE*, 1995, **2379**, 17–25.
6. Izawa, T. & Nakagome, H. Optical waveguide formed by electrically induced migration of ions in glass plates. *Appl. Phys. Lett*., 1972, **21**, 584–6.
7. Giallorenzi, T. G., West, E. J., Kirk, R., R. Ginther, R. & Andrews, R. A. Optical waveguides formed by thermal migration of ions in glass. *Appl. Opt*. 1973, **12**, 1240–5.
8. Ramaswamy, R. V. & Srivastava, R. Ion-exchanged glass waveguides: a review. *J. Lightwave Technol*., 1988, **6**, 984–1002.
9. Kilian, A., Kirchhof, J., Kuhlow, B., Przyrembel, G. & Wischmann, W. Birefringence free planar optical waveguide made by flame hydrolysis deposition (FHD) through tailoring of the overcladding. *J. Lightwave Technol*., 2000, **18**, 193–8.
10. Yliniemi, S., West, B. R. & Honkanen, S. Ion-exchanged glass waveguides with low birefringence for a broad range of waveguide widths. *Appl. Opt*., 2005, **44**, 3358–63.
11. Geraghty, D. F., Provenzano, D., Morrell, M. M., Ingenhoff, J., Drapp, B., Honkanen, S., Yariv, A. & Peyghambarian, N. Polarisation-independent Bragg gratings in ion-exchanged glass channel waveguides. *Electron. Lett*., 2000, **36**, 531–2.
12. Buchold, R. & Voges, E. Polarisation insensitive arrayed-waveguide grating multiplexers with ion-exchanged waveguides in glass. *Electron. Lett*., 1996, **32**, 2248–50.
13. Saint-André, F., Benech, P. & Kevorkian, A. P. Modellisation of a semi-leaky waveguide: application to a polariser. *Proc. SPIE*, 1991, **1583**, 278–8.
14. Honkanen, S., Pöyhönen, P. Tervonen, A. & Najafi, S. I. Waveguide coupler for potassium- and silver-ion-exchanged waveguides in glass. *Appl. Opt*., 1993, **32**, 2109–11.
15. Wang, W. J., Honkanen, S., Najafi, S. I. & Tervonen, A. Four-port guided-wave nonsymmetric Mach-Zehnder interferometer. *Appl. Phys. Lett*., 1992, **61**, 150–2.
16. Carriere, J. T. A., Ion-exchanged ring resonator integrated optic devices. Ph.D. dissertation, The University of Arizona (2004).
17. Pissadakis, S., Ikiades, A., Hua, P., Sheridan, A. K. & Wilkinson, J. S. Photosensitivity of ion-exchanged Er-doped phosphate glass using 248 nm excimer radiation. *Opt. Express*, 2004, **12**, 3131–6.
18. Geraghty, D. F., Provenzano, D., Morrell, M. M., Honkanen, S., Yariv, A. & Peyghambarian, N. Ion-exchanged waveguide add/drop filter.

Electron. Lett., 2001, **37**, 829–31.
19. Castro, J. M., Geraghty, D. F., West, B. R. & Honkanen, S. Fabrication and comprehensive modelling of ion-exchanged Bragg optical add/drop multiplexers. *Appl. Opt.*, 2004, **43**, 6166–73.
20. Auxier, J. M., Morrell, M. M., West, B. R., Honkanen, S., Schultzgen, A., Peyghambarian, N., Sen, S. & Borrelli, N. F. Ion-exchanged waveguides in glass doped with PbS quantum dots. *Appl. Phys. Lett.*, 2004, **85**, 6098–100.
21. Camy, P., Romain, J. E., Willems, F. W., Hempstead, M., van der Plaats, J. C., Prel, C., Béguin, A., Koonen, A. M. J., Wilkinson, J. S. & Lerminiaux, C. Ion-exchanged planar lossless splitter at 1·5 μm. *Electron. Lett.*, 1996, **32**, 321–3.
22. Conzone, S. D., Hayden, J. S., Funk, D. S., Roshkin, A. & Veasey, D. L Hybrid glass substrates for waveguide device manufacture. *Opt. Lett.*, 2001, **26**, 509–11.
23. Madasamy, P., Honkanen, S., Geraghty, D. F. & Peyghambarian, N. Single-mode tapered waveguide laser in Er-doped glass with multimode-diode pumping. *Appl. Phys. Lett.*, 2003, **82**, 1332–4.
24. Veasey, D. L., Funk, D. S., Peters, P. M., Sanford, N. A., Obarski, G. E., Fontaine, N., Young, M., Peskin, A. P., Liu, W.-C., Houde-Walter, S. N. & Hayden J. S. Yb/Er-codoped and Yb-doped waveguide lasers in phosphate glass. *J. Non-Cryst. Solids*, 2000, **263**, 369–81.
25. Blaize, S., Bastard, L., Cassagnètes, C. & Broquin, J. E. Multiwavelengths DFB waveguide laser arrays in Yb–Er codoped phosphate glass substrate. *IEEE Photon. Tech. Lett.*, 2003, **15**, 516–18.
26. West, B. R., Madasamy, P., Peyghambarian, N. & Honkanen, S. Modelling of ion-exchanged glass waveguide structures. *J. Non-Cryst. Solids*, 2005, **347**, 18–26.
27. Tervonen, A. A general model for fabrication processes of channel waveguides by ion exchange. *J. Appl. Phys.*, 1990, **67**, 2746–52.
28. Walker, P. G., Williamson, C. D. W. & Wilkinson, J. A. H. Integrated optical waveguiding structures made by silver ion-exchange in glass. Part 1. The propagation characteristics of stripe ion-exchanged waveguides; a theoretical and experimental investigation. *Appl. Opt.*, 1983, **22**, 1923–8.
29. Albert, J. & Lit, J. W. Y. Full modelling of field-assisted ion exchange for graded index buried channel optical waveguides. *Appl. Opt.*, 1990, **29**, 2798–804.
30. Peaceman, D. W. & Rachford, Jnr., H. H. The numerical solution of parabolic and elliptic differential equations. *J. Soc. Indust. Appl. Math.*, 1955, **3**, 28–41.
31. Frantz, J., Carriere, J., Enami, Y., Kostuk, R., Honkanen, S., Mathine, D., Peyghambarian, N., Jen, A. & Zheng, L. Optical Fibre Communications Conference, Atlanta, GA, 2003, Paper WD1.
32. Frantz, J. A., Selectively buried ion-exchanged waveguides for photonics applications. Ph.D. dissertation, The University of Arizona, 2004.
33. Stern, M. S. Semivectorial polarised finite difference method for optical waveguides with arbitrary index profiles. *IEE Proc. J.*, 1988, 135, 56–63.
34. Kim, C. M. & Ramaswamy, R. V. Modelling of graded-index channel waveguides using nonuniform finite difference method. *J. Lightwave Technol.* 1989, **7**, 1581–9.
35. West, B. R. & Honkanen, S. MMI devices with weak guiding designed in three dimensions using a genetic algorithm. *Opt. Express*, 2004, **12**, 2716–22.
36. Madasamy, P., West, B. R., Morrell, M. M., Geraghty, D. F., Honkanen, S. & Peyghambarian, N. Buried ion-exchanged glass waveguides: burial depth dependence on the waveguide width. *Opt. Lett.*, 2003, **28**, 1132–4.
37. Madasamy, P., Nunzi Conti, G., Poyhonen, P., Hu, Y., Morrell, M. M., Geraghty, D. F., Honkanen, S. & Peyghambarian, N. Waveguide distributed Bragg reflector laser arrays in erbium doped glass made by dry Ag film ion exchange. *Opt. Eng.*, 2002, **41**, 1084–6.
38. Geraghty, D. F., Castro, J., West, B. R. & Honkanen, S. All-optical packet header recognition integrated optic chip. *Proc. LEOS*, Tucson, AZ , 2004.